Effects of Cooling Time and Alloying Elements on the Microstructure of the Gleeble-Simulated Heat-Affected Zone of 22% Cr Duplex Stainless Steels

Rong-Iuan Hsieh, Horng-Yih Liou, and Yeong-Tsuen Pan

(Submitted 6 November 2000)

The effects of austenite stabilizers, such as nitrogen, nickel, and manganese, and cooling time on the microstructure of the Gleeble simulated heat-affected zone (HAZ) of 22% Cr duplex stainless steels were investigated. The submerged arc welding was performed for comparison purposes. Optical microscopy (OM) and transmission electron microscopy (TEM) were used for microscopic studies. The amount of Cr_2N precipitates in the simulated HAZ was determined using the potentiostatic electrolysis method. The experimental results indicate that an increase in the nitrogen and nickel contents raised the δ to transformation temperature and also markedly increased the amount of austenite in the HAZ. The lengthened cooling time promotes the reformation of austenite. An increase in the austenite content reduces the supersaturation of nitrogen in ferrite matrix as well as the precipitation tendency of Cr_2N. The optimum cooling time from 800 to 500 °C ($\Delta t_{8/5}$) obtained from the Gleeble simulation is between 30 and 60 s, which ensures the austenite content in HAZ not falling below 25% and superior pitting and stress corrosion cracking resistance for the steels. The effect of manganese on the formation of austenite can be negligible.

Keywords austenite, chromium carbide, chromium nitride, duplex stainless steel, ferrite, heat-affected zone

1. Introduction

Although type304 and type316 austenitic stainless steels have superior low-temperature toughness and general corrosion resistance, their pitting and stress corrosion resistances are poor in chloride-containing environments. The 22% Cr duplex stainless steels (DSS), such as UNS S31803, have superior pitting and stress corrosion resistances due to their higher pitting resistance equivalent value compared with those of type304 and type316. Therefore, DSS is extensively used in severe corrosion environments.[1]

Rong-Iuan Hsieh, Horng-Yih Liou, and **Yeong-Tsuen Pan,** Steel and Aluminum Research and Development Department, China Steel Corporation, Hsiao Kang, Kaohsiung 812, Taiwan, Republic of China. Contact e-mail: t115@mail.csc.com.tw.

On the other hand, yield strength of duplex stainless steel at room temperature is twice that of comparable γ grades and elongation is greater than 25%. This combination of properties allows DSS to be used in thinner sections than γ grades, leading to considerable savings in weight and capital investment.

The properties of DSS are dependent upon the austenite-ferrite phase ratio, which is designated to be approximately 1:1 to obtain optimum properties.[2] The phase ratio in the heat-affected zone (HAZ), however, tends to deviate from 1:1 after the weld thermal cycle. Although high heat input results in a good recovery to the phase ratio after high-temperature ferritization, low heat input leads to a limited austenite formation with detrimental consequences to its properties.

In order to possess good pitting corrosion resistance and impact energy, the HAZ of DSS requires a minimum degree of austenite reformation to avoid the formation of detrimental chromium-rich nitrides, which occur primarily in the interior of ferrite grains.[3] Although there is no specifically defined limit to ferrite content, any level exceeding 75% is unacceptable in most applications.[4] In addition, literature has reported that

Table 1 Chemical compositions of steels (wt.%)

Heat no.	C	Si	Mn	P	S*	Ni	Cr	Mo	N	Cu	B*
N1	0.013	0.48	0.89	0.020	38	5.60	22.3	3.22	0.096	0.25	28
N2	0.013	0.50	0.90	0.021	42	5.70	22.3	3.21	0.135	0.25	30
N3	0.013	0.47	0.88	0.021	48	5.50	22.3	3.07	0.150	0.22	25
N4	0.013	0.48	0.89	0.020	38	5.60	22.3	3.22	0.165	0.25	28
Ni1	0.013	0.48	0.88	0.021	44	4.57	22.3	3.16	0.155	0.24	28
Ni2	0.013	0.48	0.88	0.021	44	6.57	22.3	3.16	0.155	0.24	28
Mn1	0.021	0.47	0.95	0.024	59	5.45	22.3	3.09	0.145	0.22	25
Mn2	0.021	0.47	1.5	0.024	59	5.45	22.3	3.09	0.145	0.22	25

* Content in ppm

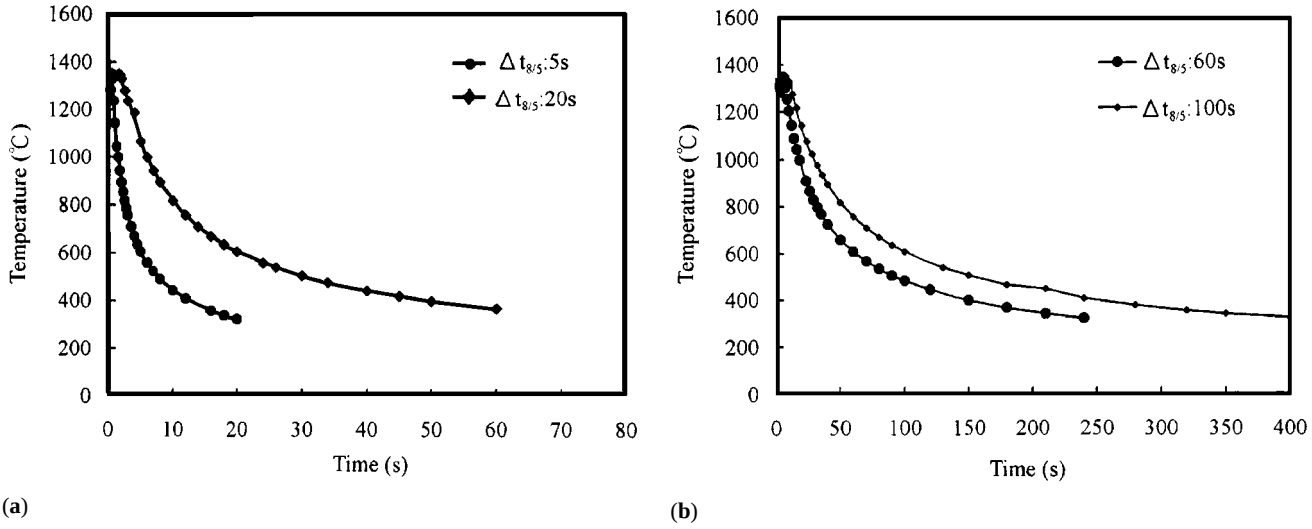

Fig. 1 Thermal history of the Gleeble simulation: (**a**) $\Delta t_{8.5}$: 5 and 20 s; and (**b**) $\Delta t_{8.5}$: 60 and 100 s

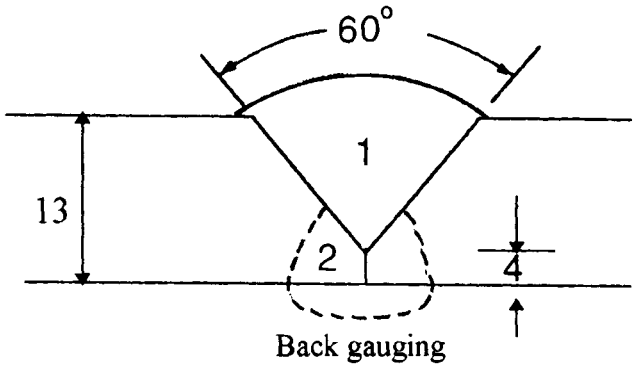

Fig. 2 Schematic of joint preparation for SAW

Table 2 Parameters for SAW in each pass

Current (A)	Arc voltage (A)	Travel speed (cm/min)	Heat input (KJ/cm)	$t_{8/5}$ (s)
450	34	35	26	60

$t_{8/5}$: cooling time from 800 to 500 °C

modern duplex steels normally show ferrite levels in the HAZ in the range of 50 to 70% if appropriate welding conditions are used.[5] Thus, it is apparent that welding parameters should be specified to ensure that the overall cooling conditions are slow enough to allow adequate austenite formation within the high-temperature regions yet fast enough to avoid deleterious precipitation in the low-temperature regions. The guideline is given by the cooling times between 800 and 500 °C, $\Delta t_{8/5}$, which is typically the temperature range within which austenite formation occurs.[6]

The purposes of this study are to evaluate the effects of austenite stabilizers, such as nitrogen, nickel, and manganese, and of the cooling times from 800 to 500 °C ($\Delta t_{8/5}$) after welding on the reformation of austenite and the tendency of Cr_2N precipitation. Furthermore, a submerged arc welding was carried out to compare the HAZ microstructures under the Gleeble simulation and real welding.

2. Experimental Procedure

The experimental steels were prepared from 250 kg vacuum-melted heats and cast into 160 by 160 mm square ingots. Table 1 lists the chemical compositions of the experimental steels with base composition remaining 0.02% C-0.48% Si-0.021% P-22.3% Cr-3.2% Mo-0.25% Cu-28 ppm B, with a variant designed using variations of nitrogen, nickel, and manganese contents. The steels were reheated at 1240 °C for 1 h and hot rolled to a 13 mm thickness. Before simulation and real welding, these steels were subjected to solution treatment at 1100 °C for 10 min and then quenched in cold water.

Longitudinal specimens 10.5 × 10.5 × 80 mm^3 were cut from the plate and subjected to HAZ simulation with a Gleeble 1500 thermomechanical simulator. The thermal history of the simulation was based on a temperature/time function derived by Hannerz,[6] where the peak temperature of 1350 °C was held for 1 s, and where the cooling times from 800 to 500 °C ($\Delta t_{8/5}$) were 5, 20, 60, and 100 s, respectively. Figure 1 shows the thermal history for the Gleeble simulation with the relationship between $\Delta t_{8/5}$ and the arc energy[6] being as follows:

$$Q/d = K \times (\Delta t_{8/5})^{1/2} \quad [1]$$

where

Q = net heat input (J/mm),
d = thickness (mm),
K = coefficient (J/mm^2·s$^{1/2}$) (about 25.52 for duplex stainless steel),
$\Delta t_{8/5}$ = cooling time from 800 to 500 °C (in s).

The HAZ microstructure was examined using optical microscopy and transmission electron microscopy (TEM). Quantitative measurements of the austenite phase content and

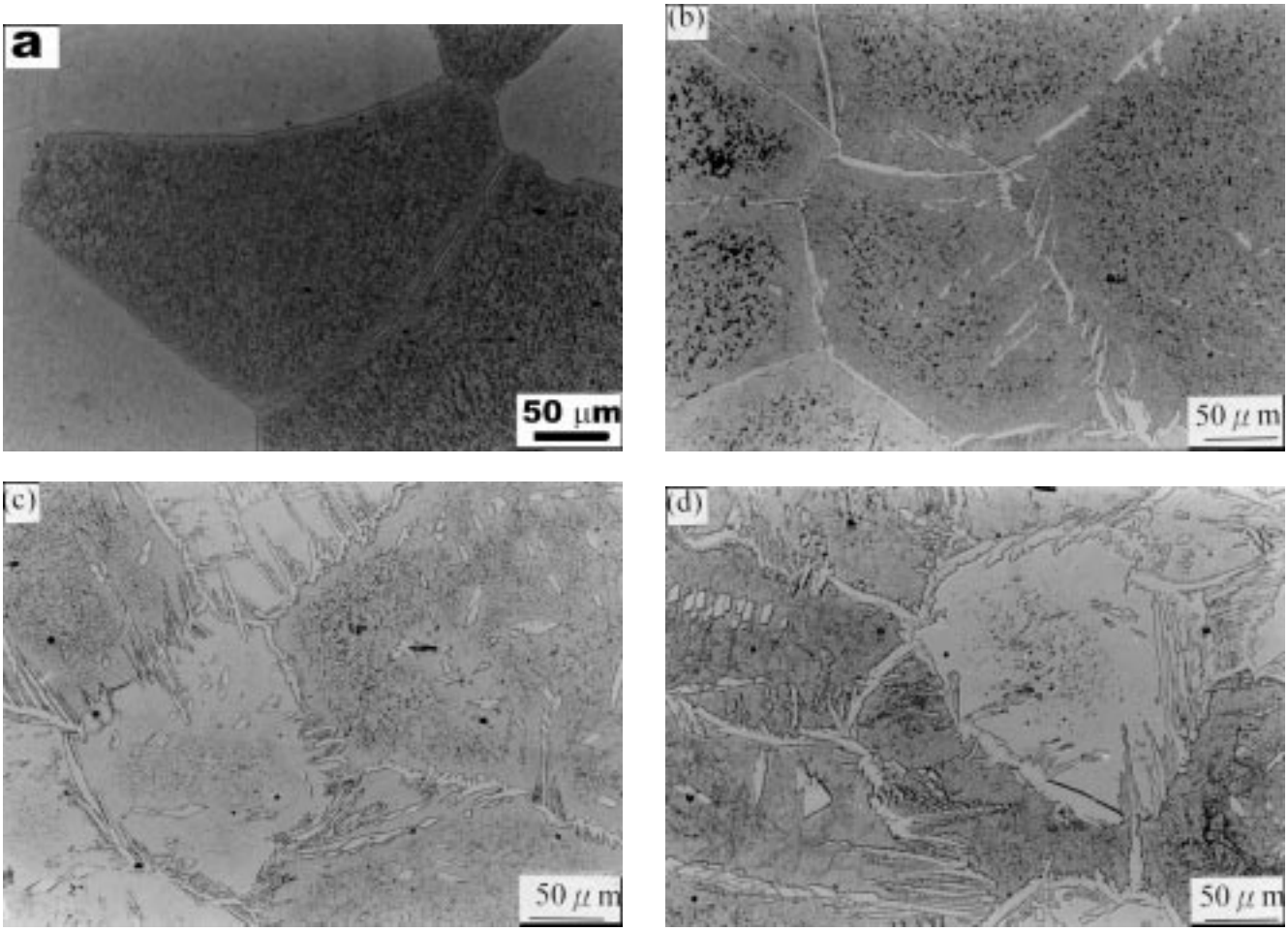

Fig. 3 Microstructures in the simulated HAZ of 0.1% N steel at various cooling rates: (**a**) $\Delta t_{8.5}$: 5 s; (**b**) $\Delta t_{8.5}$: 20 s; (**c**) $\Delta t_{8.5}$: 60 s; and (**d**) $\Delta t_{8.5}$: 100 s

ferrite grain size were carried out using point counting and mean linear intercept methods with magnifications of 800 and 200×, respectively, with the area examined being about 4 mm^2. In addition, the insoluble nitrogen content of simulated HAZ was determined by analyzing the nitrogen content of precipitates. Extraction of the precipitates from the simulated HAZ was performed by potentiostatic electrolysis in which a specimen within dimensions of 10.5 × 10.5 × 3 mm^3 was immersed into an electrolyte and dissolved electrochemically until a weight loss of about 0.6 to 0.7 g was achieved. The electrolyte was prepared by adding 50 g of tetraethyl ammonium chloride into 500 mL acetyl acetone and diluting this with methyl alcohol to 5000 mL. The precipitates were filtered using a filter with 2 μm pore size. The precipitate nitrogen content in ppts was then determined using inductively coupled plasma optical emission spectrometry.

The submerged arc welding (SAW) was performed to compare the microstructures under the Gleeble simulation and real welding. The steels used in the real welding contained a variety of nitrogen levels, as shown in Table 1. The joint preparation is shown in Fig. 2. After the first pass was finished, back gouging was performed, and a second pass made. The consumable for the SAW test was consistent with the standards of AWS A 5.9 with the welding conditions being shown in Table 2.

3. Results and Discussion

3.1 Effects of Gleeble Simulation Cooling Time on Microstructure

Figure 3 shows the effect of cooling time on the simulated microstructure for 0.1% N-5.5% Ni steel, indicating that the dominant microstructure in the HAZ is of the ferrite phase with a little grain boundary austenite (GBA) when the cooling time is limited to 5 s. The Widmanstätten type and intragranular austenite can be observed with increasing cooling time, which significantly promotes the austenite formation. Literature shows that the diffusion distance of nitrogen is 50 to 100 μm during a weld thermal cycle, which is much longer than those of chromium and nickel, 0.5 and 2 μm, respectively.[7] The precipitation of austenite is a diffusion-controlled nucleation and growth process, and, at least in low arc energy welds, the austenite reformation is controlled by a paraequilibrium transformation mechanism in which the diffusion of the interstitial elements (carbon and nitrogen) is the controlling process.[8,9]

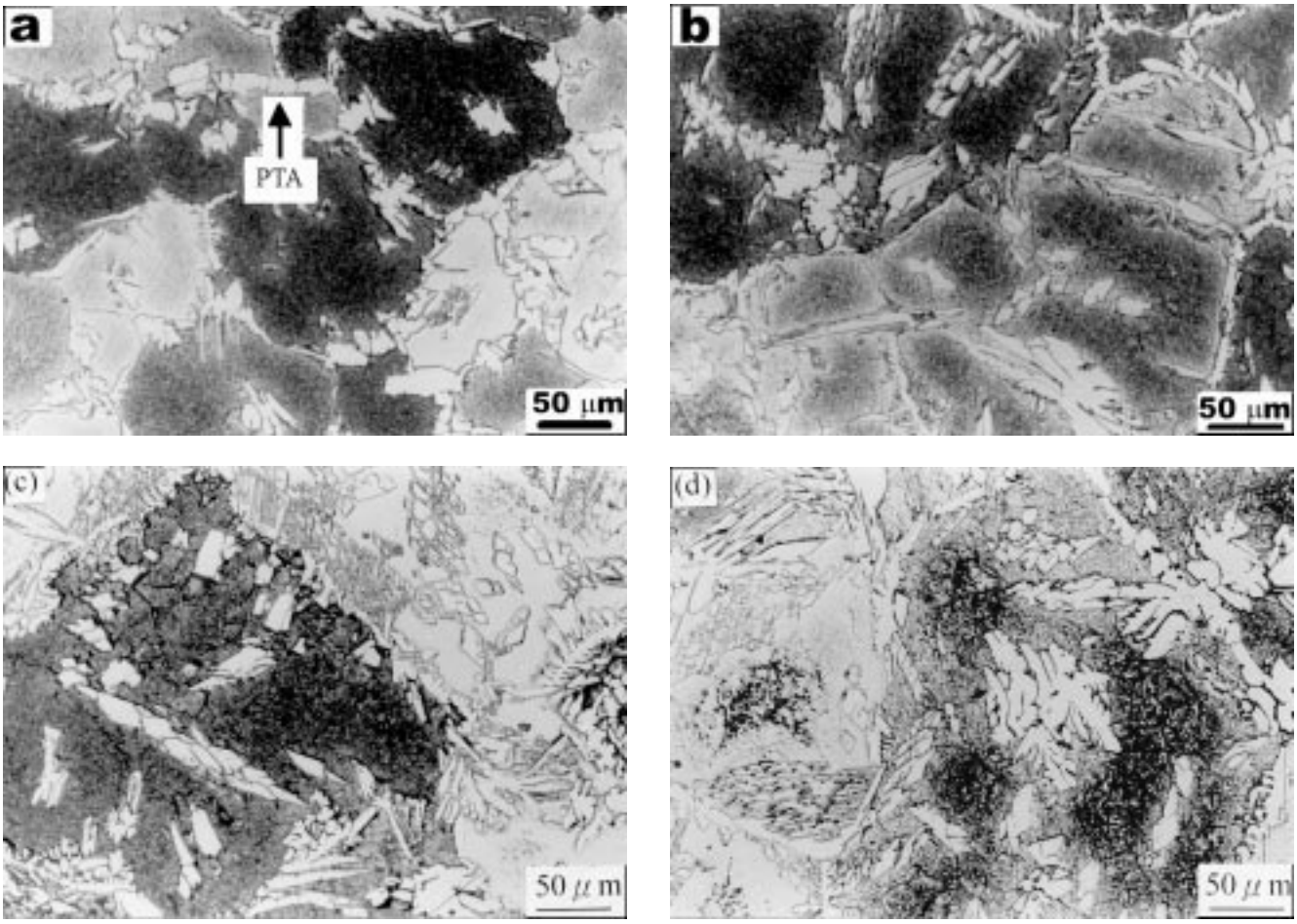

Fig. 4 Microstructures in the simulated HAZ of 0.165% N steel at various cooling rates: (**a**) $\Delta t_{8.5}$: 5 s; (**b**) $\Delta t_{8.5}$: 20 s; (**c**) $\Delta t_{8.5}$: 60 s; and (**d**) $\Delta t_{8.5}$: 100 s

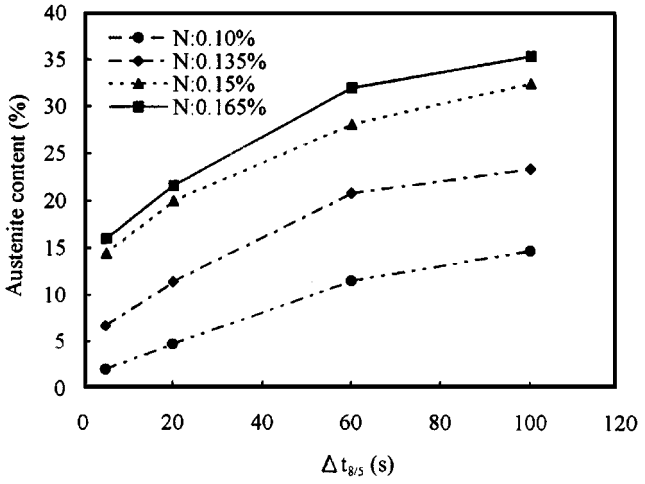

Fig. 5 Variation of austenite content with cooling time at various nitrogen contents

Thus, the cooling rate is very important in determining the extent of austenite formation. Slow cooling rates result in more austenite, while fast cooling rates give less austenite. The grain growth of ferrite observed in Fig. 3 will be discussed in Section III–C.

Figure 4 shows the effect of cooling time on the simulated HAZ microstructure for 0.165% N-5.5% Ni steels. Comparing Fig. 3 and 4, it is clear that not only the austenite content has increased markedly, but also the ferrite grain size is finer, showing that, just as the nucleation of austenite is facilitated at grain boundaries, a small ferrite grain size favors a high austenite content. In addition to the Widmanstätten, intragranular, and GBA types, the partially transformed austenite (PTA) at shortened cooling time can also be found, as shown in Fig. 4(a). The literature also reports that the austenite phase in the HAZ of DSS can be classified as reformed austenite and PTA,[10] respectively.

The austenite phase reformation in the HAZ occurs during the cooling stage. Under a fast cooling process, the austenite reforms on the ferrite grain boundaries with a blocky morphology; yet, when the cooling rate is decreased, the Widmanstätten type austenite precipitates from the ferrite grain boundaries into the interior of the grains. Moreover, when the banded austenite phase in the original base metal is subjected to rapid heating in the HAZ, a partial ferritization of the austenite phase is often observed. When these untransformed austenites are again

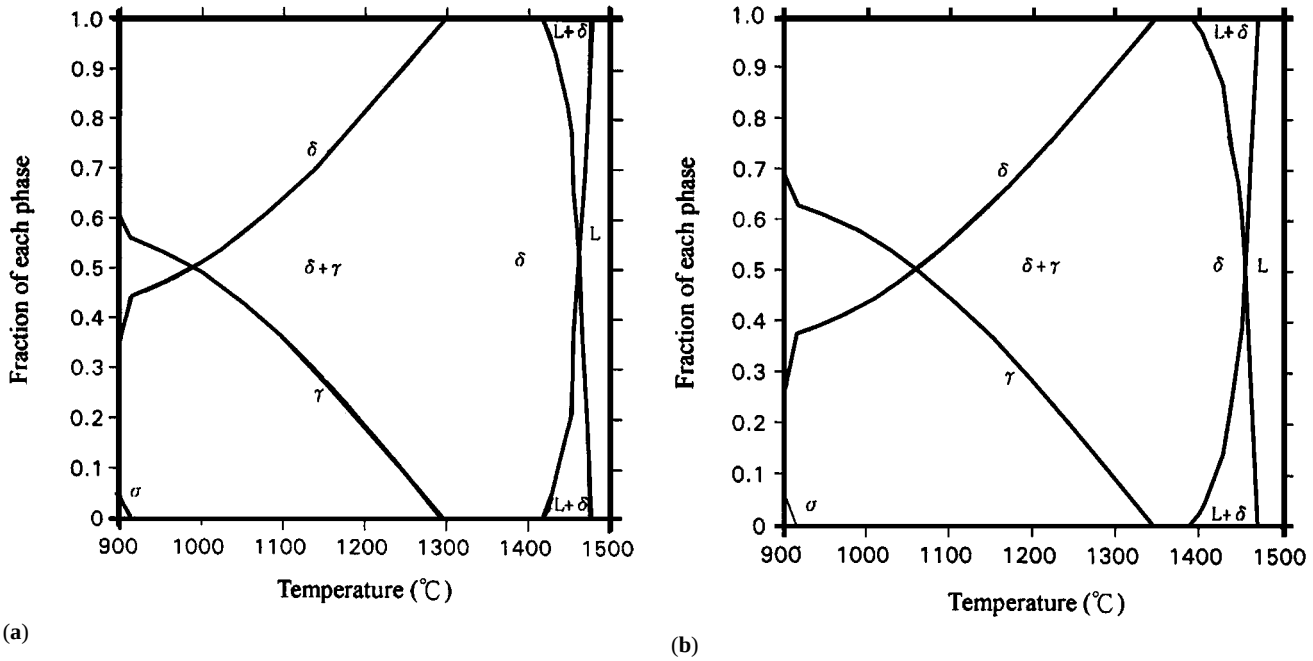

Fig. 6 Calculated equilibrium fractions of phases vs temperature at various nitrogen contents: (**a**) 0.1% N and (**b**) 0.165% N

subjected to fast cooling, they still retain a banded structure and are termed as PTA. The PTA can pin the ferrite grain boundary and inhibit further grain growth.[10] Similar results have been found in this work.

3.2 Effect of Alloying Elements on the Formation of Austenite

Figure 5 shows the relationship between cooling time and austenite content under various nitrogen contents, from which it can be seen that the austenite content significantly increases with increasing nitrogen content at any given cooling time. Because the precipitation of austenite starts below the ferrite solvus temperature (A_4 temperature), which, in turn, is dependent on the composition of the steel plate. A higher nitrogen content in the steel plate will raise the A_4 temperature and enhance the austenite reformation. The austenite content in the HAZ may be selected as a criterion for ensuring superior pitting, stress corrosion cracking resistance, and mechanical properties.

In general, an austenite content of more than 25% is suggested.[4] To satisfy this criterion, the nitrogen content of the steel and the cooling time ($\Delta t_{8/5}$) should be above 0.145% and 40 s, respectively. The effect of nitrogen content on the phase equilibrium in the Fe-22.3Cr-3.2Mo-5.5Ni system was calculated using Thermo-Calc software[11] and shown in Fig. 6. Approximately equal volume fractions of austenite and ferrite are obtained at 950 °C for 0.10% N steel (Fig. 6a); however, the volume fraction of austenite decreases with increasing temperature, and, since the full dissolution of austenite occurs at about 1300 °C, a single phase ferrite forms and becomes coarse under the test temperature of 1350 °C (as shown in Fig. 3).

In contrast, approximately equal volume fractions of austenite and ferrite are obtained at 1050 °C for 0.165% N steel (Fig. 6b); the temperature for full austenite dissolution rises to about 1360 °C, which is 60 °C higher than that of 0.1% N steel.

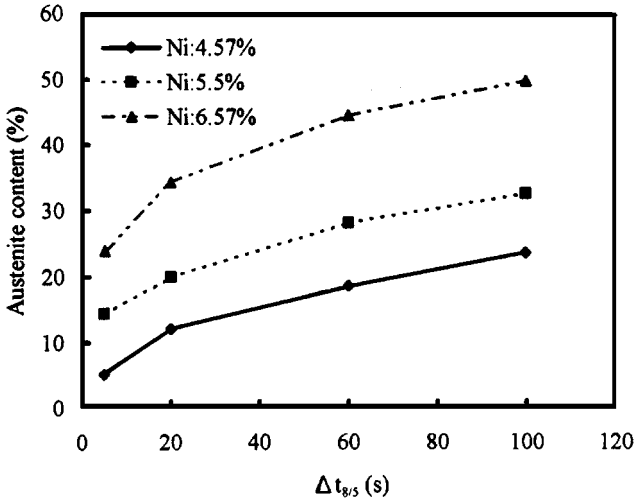

Fig. 7 Austenite content as a function of cooling time at various nickel contents

Consequently, one can still find PTA at the test temperature of 1350 °C, and, with PTA inhibiting the coarsening of ferrite, the ferrite grain size of 0.165% N steel is finer (Fig. 4). Furthermore, as the nucleation of austenite is preferred at grain boundaries, the small ferrite grain size enhances the well-placed reformation of austenite. Accordingly, the increase of austenite content with increasing nitrogen content can be seen as being due to the increased A_4 temperature and refined ferrite grains.

Figure 7 shows the relationship between cooling time and austenite content under a variety of nickel contents, and it is evident that the austenite content rises dramatically with the increase of nickel content. However, to reach 25% austenite requirement in the HAZ, the nickel content of the steel and the

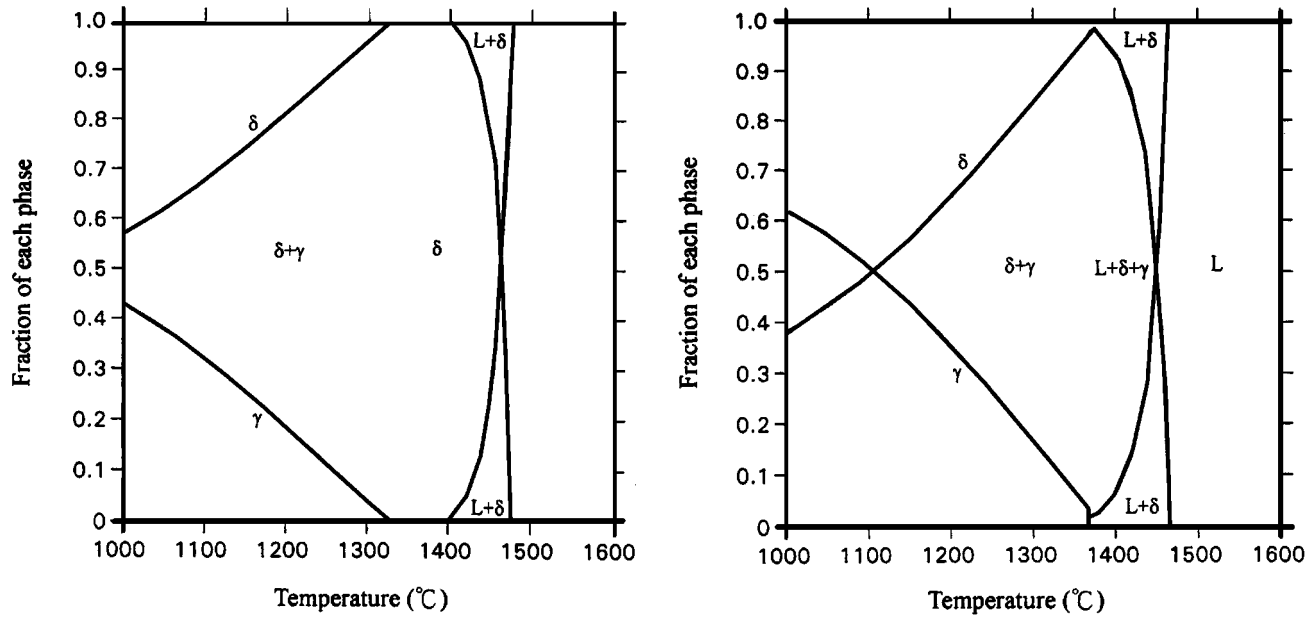

(a) (b)

Fig. 8 Calculated equilibrium fractions of phases vs temperature at various nickel contents: (**a**) 4.5% Ni and (**b**) 6.5% N

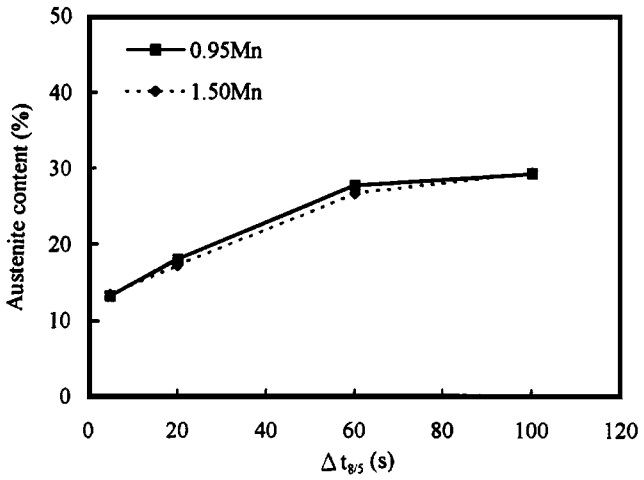

Fig. 9 Variation of austenite level with cooling time at various manganese contents

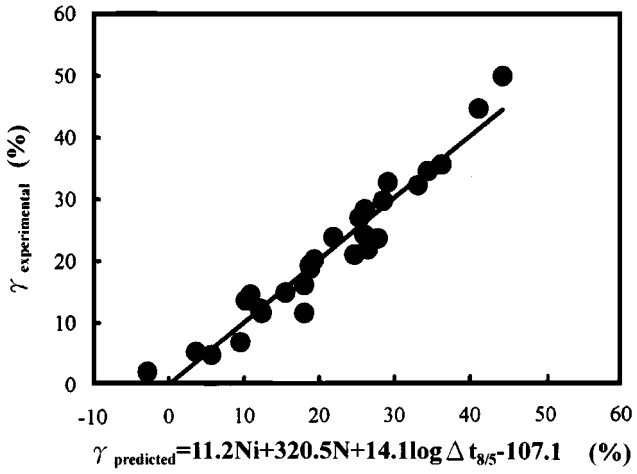

Fig. 10 A comparison of the experimental and predicted austenite contents in the simulated HAZ

cooling time ($\Delta t_{8/5}$) should be above 5.5% and 50 s, respectively. This implies that the potential of nickel to promote the reformation of austenite is somewhat weaker than that of nitrogen. The effect of nickel content on the phase equilibrium in the Fe-22.3Cr-3.2Mo-0.15N system was calculated[11] and shown in Fig. 8. The temperature for full austenite dissolution is about 1320 °C for 4.5% Ni steel. However, the dissolution temperature of austenite rises to 1370 °C when the nickel content is increased to 6.5%. As nickel is an austenite former, the austenite content naturally increases with an increasing nickel content, which raises A_4 temperature and the refinement of the ferrite grains.

Figure 9 shows the relationship between the cooling time and the austenite content at various manganese contents. The effect of manganese on the formation of austenite is only minor. The literature shows that manganese has little effect on duplex phase balance, especially in the content normally encountered,[12] and similar results have also been found in this study.

Figure 10 shows the result of regression analysis to compare the effects of austenite formers and cooling time on the austenite content under simulated HAZ conditions. The effects of austenite stabilizer and cooling times on the austenite level can be expressed by the following equation:

$$\gamma = -107.1 + 320 \times \mathrm{N} + 11.2 \times \mathrm{Ni} + 14.1 \times \log \Delta t_{8/5} \quad [2]$$

where

γ = austenite content (vol.%),
$\Delta t_{8/5}$ = cooling time from 800 to 500 °C (s), and
N, Ni = nitrogen and nickel content (wt.%).

It is obvious that nitrogen has a much greater effect on the reformation of austenite than nickel. Although both nitrogen and nickel are austenite formers, the diffusion coefficients of nitrogen and nickel in the ferrite at high temperature are about 1.3×10^{-6} and 3.9×10^{-11} cm^2/s,[7] respectively. These show that the diffusion of nitrogen is much faster than that of nickel, and, therefore, the effect of nitrogen on promoting the reformation of austenite is greater. Concerning the cooling time after welding, using higher heat input for decreasing cooling time favors the diffusion of alloying elements and increases the austenite content. In addition, the selection of an appropriate heat input is also important to ensure superior corrosion resistance and mechanical properties in the HAZ of 22% Cr DSS.

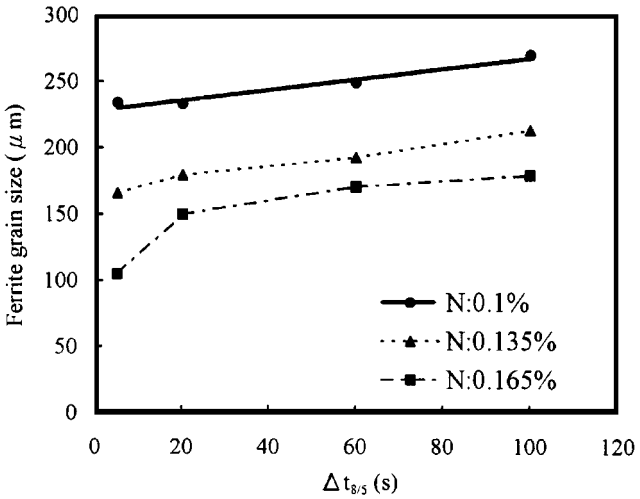

Fig. 11 Ferrite grain size as a function of cooling time at various nitrogen contents

In general, the chromium-rich nitride, specifically Cr_2N, is observed when the HAZ has a high proportion of ferrite. This is due to the lower solubility of nitrogen in ferrite. However, the precipitation of $Cr_{23}C_6$ or σ phase can take place when the cooling time is too long.[13,14] Since both cases will deteriorate the properties of HAZ, an intermediate heat input is suggested for the welding of 22% Cr DSS.

3.3 Ferrite Grain Size

Figure 11 shows the ferrite grain size as a function of cooling time at various nitrogen contents, indicating grain size reduction with decreasing cooling time and increasing nitrogen content. However, the effect of nitrogen content on the grain size is more evident than that of cooling time. The grain size of 0.1% N and 0.165% N steels increases from 230 to 270 μm and from 100 to 150 μm, respectively, when the cooling time rises from 5 to 100 s. Figure 12 shows the change of microstructure in the simulated HAZ of 0.1% N steel at a cooling time of 5 s. The morphology of austenite, which is uniformly distributed in the ferrite matrix in base metal, is stringerlike, and such austenite began to dissolve when the temperature of the Gleeble simulation exceeded 950 °C (Fig. 6a and 12), and fully dissolved to form a single ferrite phase when the temperature reached 1350 °C. The ferrite grains markedly coarsened due to the absence of any pinning effect from the austenite.

The change of microstructure in the simulated HAZ of 0.165% N at a cooling time of 5 s is shown in Fig. 13. Comparing Fig. 12 and 13, it is clear that the ferrite grain size of 0.165% N steel is finer than that of 0.1% N steel. On the other hand, the morphology of austenite in 0.165% N steel has a banded structure, which begins to dissolve when the simulation temperature exceeds 1050 °C (Fig. 6b and 13). However, one can still find PTA, as shown in Fig. 13, even if the simulation temperature reaches 1350 °C. These undissolved austenite particles can pin the ferrite grain boundary and inhibit grain growth. Atamert *et al.*[10] reported that the ferrite grain growth is very sensitive to the initial banded austenite structure of the base metal, which in turn affects the PTA in the HAZ. The PTA pins the ferrite

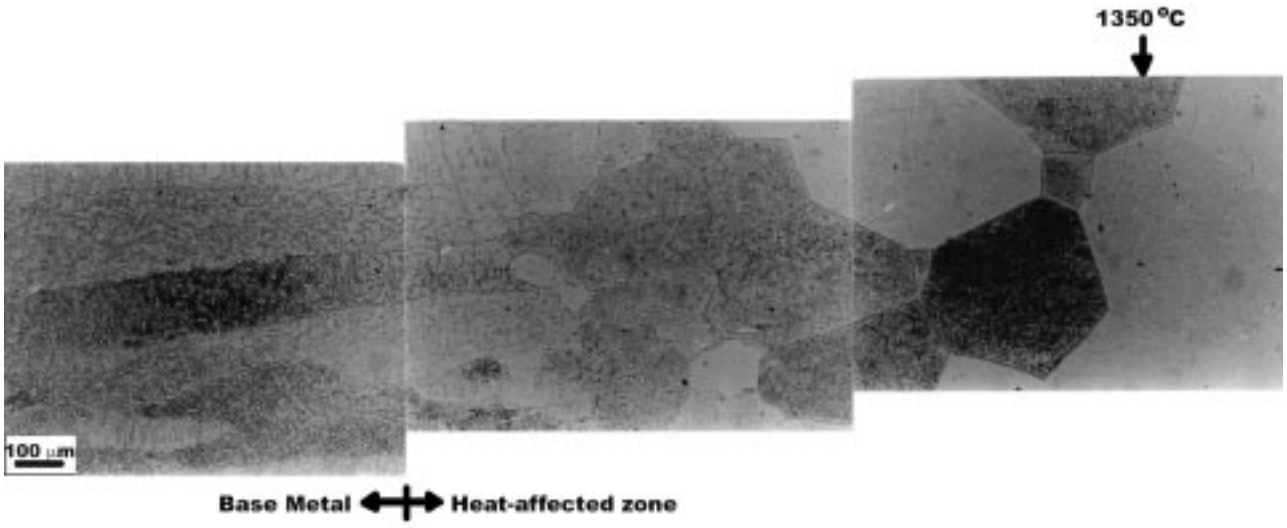

Fig. 12 Microstructural changes in the simulated HAZ for 0.1% N steel at $t_{8/5}$: 5 s.

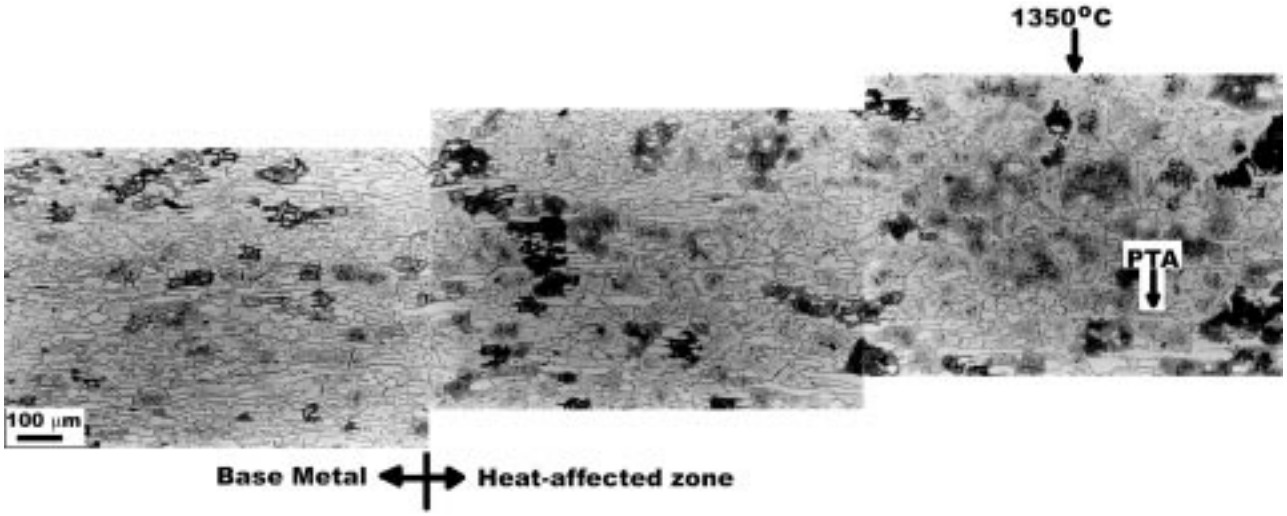

Fig. 13 Microstructural changes in the simulated HAZ for 0.165% N steel at $t_{8/5}$: 5 s.

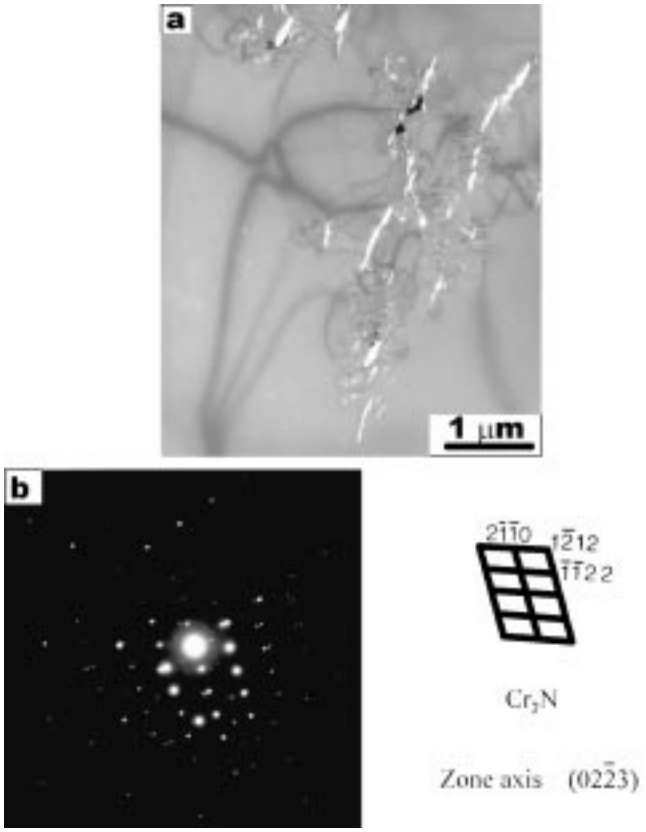

Fig. 14 Electron microscopy of intragranular precipitates in the simulated HAZ of 0.1% N steel at $t_{8/5}$: 5 s.: (**a**) dark-field image and (**b**) diffraction pattern

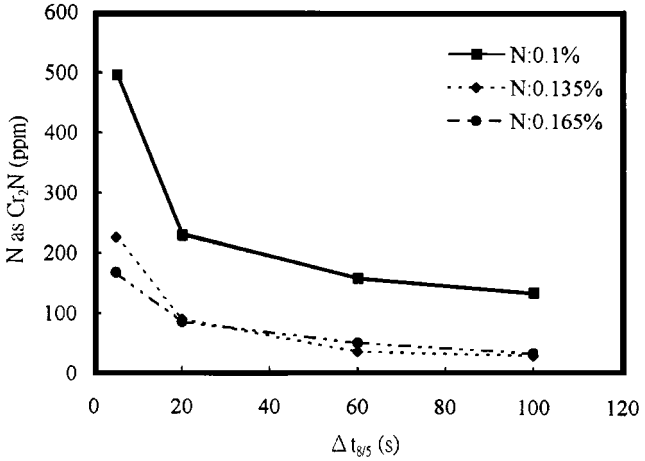

Fig. 15 Effect of cooling time on the nitride precipitation in the simulated HAZ at various nitrogen contents

3.4 Effect of Cooling Time and Alloying Elements on Precipitation of Cr_2N

Figure 14 shows the TEM micrograph of a simulated HAZ for 0.10% N-5.5% Ni steel at a cooling time of 5 s. The precipitation of Cr_2N with size ranging from 0.1 to 0.5μm is observable in the ferrite matrix. From an optical micrograph, as shown in Fig. 3(a), the ferrite content in this specimen reached 97%, which resulted in the supersaturation of nitrogen in ferrite and promoted the precipitation of Cr_2N. Figure 15 shows the effect of cooling time on the nitrogen in the form of Cr_2N precipitates under various steel plate nitrogen contents. The nitrogen in the form of Cr_2N precipitates markedly increases with a decreasing steel plate nitrogen content and a shortened cooling time.

Figure 16 shows the effect of cooling time on the nitrogen content in the form of Cr_2N precipitates under various nickel contents. The nitrogen in the form of Cr_2N significantly declined with the increasing nickel content and lengthened cooling time. The supersaturation of nitrogen in the ferrite decreased with

grain boundary and prevents grain growth. Similar results have been found in this work, though for short cooling times, the PTA caused small ferrite grain sizes, whereas for longer cooling times, the residual amount of PTA became less and less, and therefore lost its pinning effect.

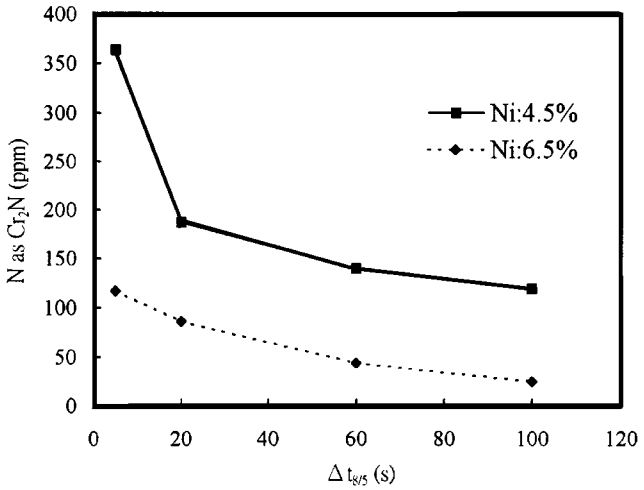

Fig. 16 Effect of cooling time on the nitride precipitation in the simulated HAZ at various nickel contents

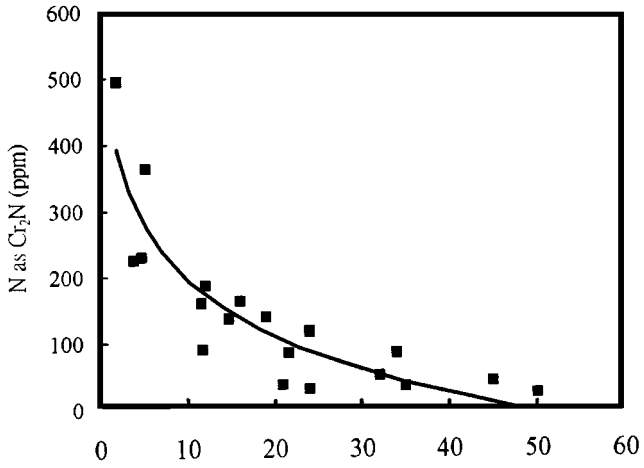

Fig. 17 Relationship between austenite content and amount of nitride precipitate in the simulated HAZ

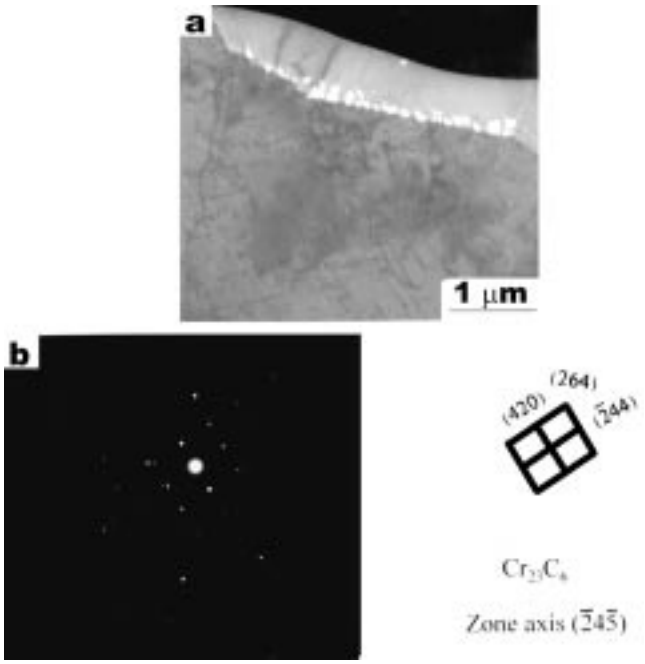

Fig. 18 Electron microscopy of grain boundary precipitates in the simulated HAZ of 0.1% N steel at $t_{8/5}$: 100 s: (**a**) dark-field image and (**b**) diffraction pattern

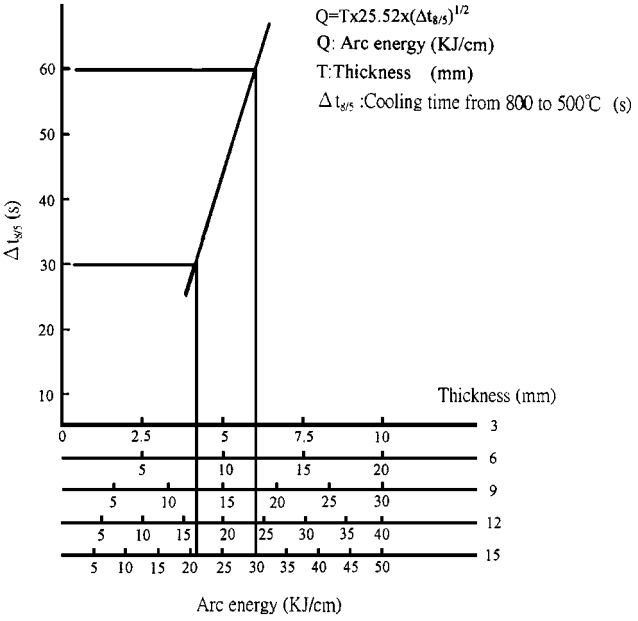

Fig. 19 Nomogram for the prediction of arc energy from $t_{8/5}$: for 22% Cr duplex stainless steels

the increasing austenite content and the longer cooling time, and it also decreased the precipitation of Cr_2N. Figure 17 shows the effect of austenite content on the nitrogen in the form of Cr_2N. The higher the austenite content, the lower the nitrogen in the form of Cr_2N. The concentration of nitrogen in Cr_2N fell below 100 ppm when the austenite content exceeded 25%. The solubility of nitrogen in austenite is as high as 2.8%, which is much higher than that in ferrite, and this accounts for the decrease in Cr_2N precipitation.[15]

Previous literature shows that the precipitation of Cr_2N will highly decrease the pitting and stress corrosion resistance.[16] However, the pitting and stress corrosion resistance can be maintained when the austenite content does not fall below 25% due to the decrease of the precipitation of Cr_2N. Accordingly, an increase of cooling time after welding will promote the reformation of austenite under suitable nitrogen and nickel contents, and prevent Cr_2N precipitation. Conversely, with nitrogen and nickel contents lower than 0.15 and 5.5%, respectively, the reformation of austenite is limited, even if the cooling time is increased, and will result in the formation of Cr_2N. On the other hand, when the cooling time is over 80 s, $Cr_{23}C_6$ will precipitate at the grain boundary, as shown in Fig. 18. According to the experimental results, the alloy design and the cooling time are the key points to assure that the austenite content in the HAZ does not fall below 25% and to avoid precipitation

of Cr_2N, guaranteeing superior pitting and stress corrosion resistance at the HAZ.

The most suitable cooling time ($\Delta t_{8/5}$) obtained from the Gleeble simulation was found to be between 30 and 60 s for 0.165% N-5.5% Ni-22.3% Cr-3.2% Mo duplex stainless steel. Furthermore, these cooling times can be related to arc energy for any given material thickness from monograms, such as that shown in Fig. 19.

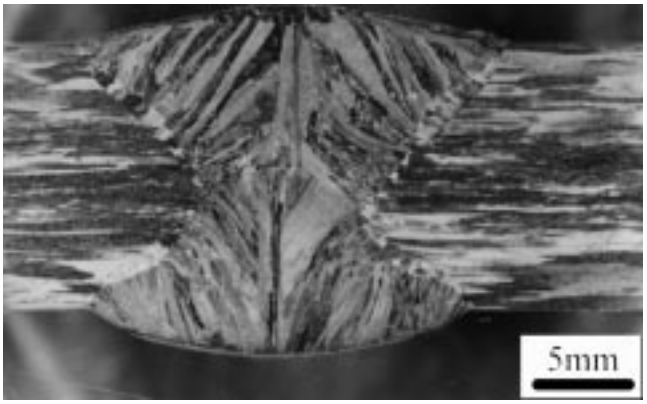

Fig. 20 Macrograph of the submerged arc weldment

3.5 Results of SAW

Figure 20 shows the macrograph of the SAW. Weld appearance is even and no defect is observable. Figure 21 shows the microstructure of welds at various nitrogen contents. It is clear that, in addition to the increase of austenite content, the width of the HAZ is narrower and the ferrite grain size finer with an increasing nitrogen content of the steel plate. Figure 22 shows the difference in austenite content between the Gleeble simulation and a real welding HAZ. The austenite content in the Gleeble simulated HAZ is higher than that of a real welding by about 3%. This is because the peak temperature in the Gleeble simulated HAZ was set at 1,350 °C, which is 50 °C lower than that measured in a real welding. It has been reported that the higher the peak temperature, the lower the austenite content in the HAZ, due to the ferrite grain size being coarsened with increasing peak temperature, so that a large ferrite grain size has a retarding effect on austenite reformation.[17] Table 3 shows the mechanical properties of the weld. Both the tensile and the bending tests meet the specification requirements. From the experimental results, it is clear that the suitable cooling time established using the Gleeble simulation could be used as a reference in the selection of welding conditions during the joining of 22% Cr duplex stainless steels.

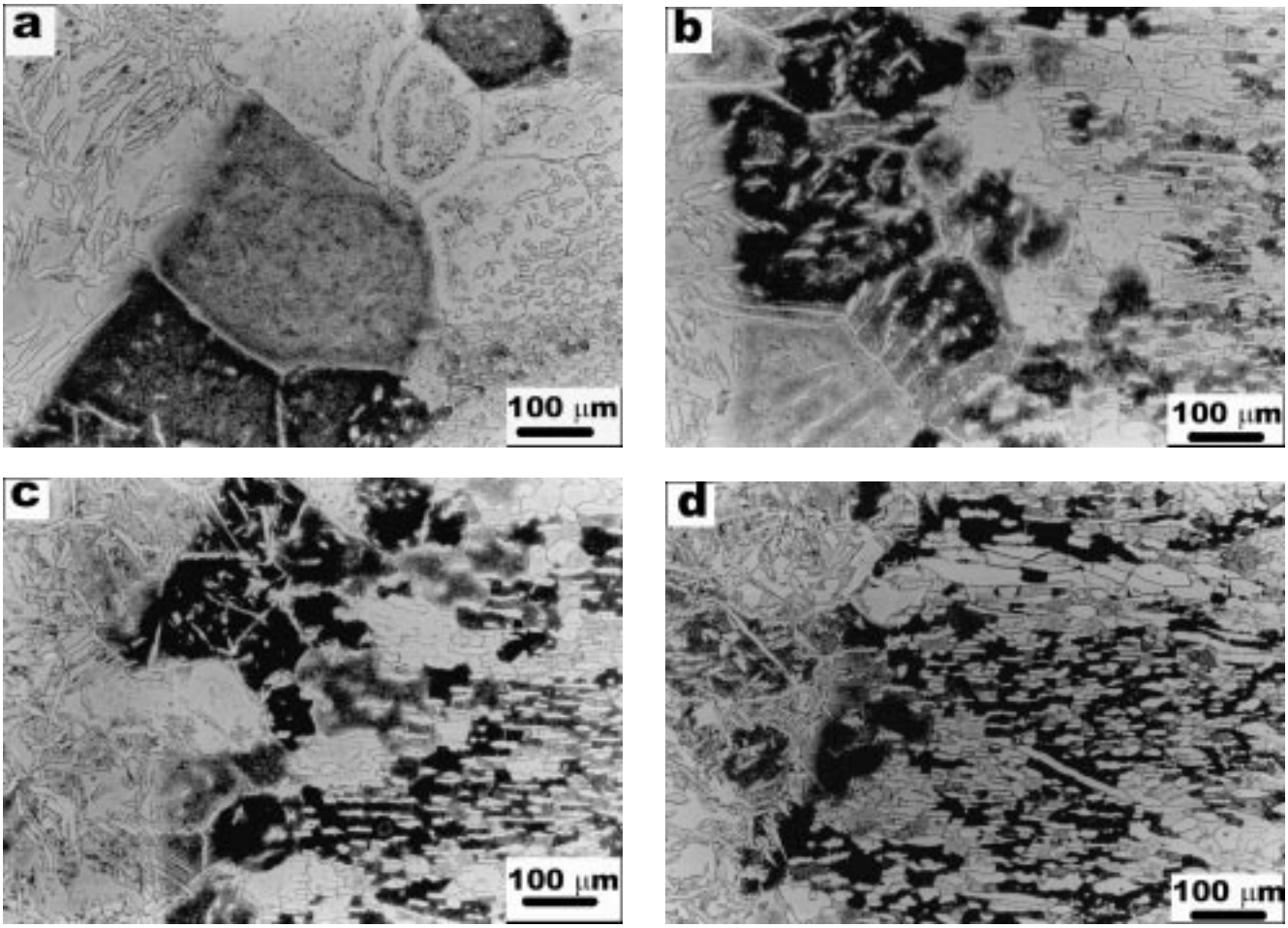

Fig. 21 Microstructures of welded joint at various nitrogen contents: (**a**) 0.1% N, (**b**) 0.135% N, (**c**) 0.15% N, (**d**) 0.165% N

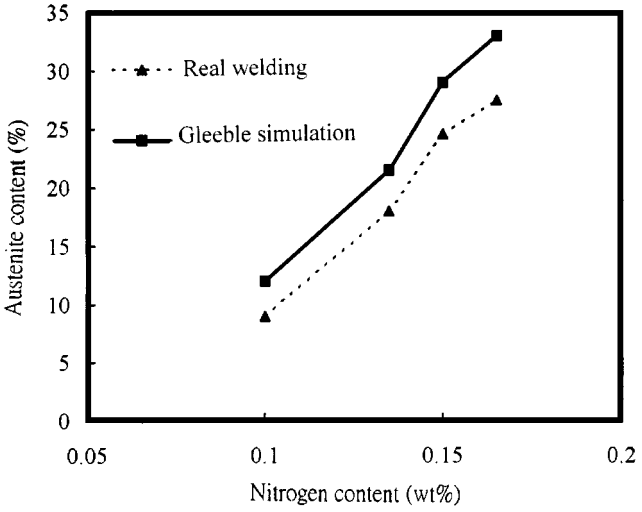

Fig. 22 Comparison of austenite content from the Gleeble simulation and a real welding HAZ at various nitrogen contents.

Table 3 Mechanical properties of weldment

Heat no.	Face bending ($R = T$)	Back bending ($R = T$)	Side bending ($R = T$)	Yield strength (MPa)	Tensile strength (MPa)	Elongation (%)	Fracture position
N1	…	…	…	574.3	765.0	28.8	Base metal
N2	OK	OK	OK	593.4	770.6	33.1	Base metal
N3	…	…	…	574.4	763.7	31.7	Base metal
N4	…	…	…	585.1	765.1	32.5	Base metal

4. Summary and Conclusions

The Gleeble simulation was carried out to evaluate the effect of alloying elements and cooling time on the reformation of austenite in the HAZ. In addition, the SAW was performed to compare the HAZ microstructures under the Gleeble simulation and a real welding. The main conclusions drawn were as follows.

- The cooling time after welding has a significant effect on the reformation of austenite in the HAZ. Increased cooling time favors diffusion of alloying elements and promotes the reformation of austenite.
- Both nitrogen and nickel are effective austenite formers. Increasing their contents greatly promotes the reformation of austenite. However, the effect of the nitrogen on the reformation of austenite is much greater than that of nickel.
- The effect of austenite stabilizers and cooling times on the austenite content in the HAZ is summarized using the following linear regression:

$$\gamma(\%) = 320.5 \times \mathrm{N} + 11.2 \times \mathrm{Ni} + 14.1 \times \log \Delta t_{8/5} - 107.1$$

- Any decrease in the austenite former and/or the cooling time after welding results in a high proportion of ferrite in the HAZ, which leads to a supersaturation of nitrogen and enhances the precipitation of Cr_2N.
- The optimum cooling time ($\Delta t_{8/5}$) after welding is between 30 and 60 s for 0.165% N-5.5% Ni-22.3% Cr-3.2% Mo duplex stainless steel. All cooling times can be computed to arc energy for any given material thickness.
- The differences in austenite content between the Gleeble simulation and a real welding are relatively small for the same cooling times. Therefore, the cooling time established by the Gleeble simulation can be successfully used as a reference in the selection of welding conditions during the joining of 22% Cr duplex stainless steels.
- The effect of manganese on the formation of austenite can be negligible.

References

1. T. Kudo, H. Tsuge, and T. Moroishi: *Corr. J.*, 1989, vol. 45, p. 831.
2. W.A. Baeslack and J.C. Lippold: *Met. Const.*, 1988, vol. 20, p. 26R.
3. L. Karlsson, L. Ryen, and S. Pak: *Weld. J.*, 1995, vol. 74, p. 28.
4. R.M. Davison and J.D. Redmond: *Mater. Selection Design*, 1990, vol. 11, p. 57.
5. T. Omura, T. Kushida, T. Kudo, T. Hayashi, Y. Matsuhiro, and T. Hikida: *Tetsu-to-Hagané*, 1997, vol. 83, p. 37.
6. B.E.S. Lindblom, B. Lundquivst, and N. Hannerz: *Scand. J. Metall.*, 1991, vol. 20, p. 305.
7. G.L. Leone and H.W. Kerr: *Weld. J.*, 1982, vol. 61, p. 13.
8. N. Suutala, T. Talkalo, and T. Moisio: *Metall. Trans. A*, 1980, vol. 11A, p. 717.
9. S. Hertzman, P.J. Ferreira, and B. Brolund: *Metall. Mater. Trans. A*, 1997, vol. 28A, p. 277.
10. S. Atamert and J.E. King: *Mater. Sci. Technol.*, 1992, vol. 8, p. 896.
11. B. Sundman, B. Jansson, and J.O. Andersson: *CALPHAD*, 1985, vol. 9, p. 153.
12. R.N. Gunn: *Duplex Stainless Steels—Microstructure, Properties and Applications*, Woodhead Publishing Ltd., Cambridge, United Kingdom, 1997.
13. H. Tsuge, Y. Tarutani, and T. Kudo: *Corr. J.*, 1988, vol. 44, p. 305.
14. M.J. Huh, S.B. Kom, K.W. Paik, and Y.G. Kim: *Scripta Mater.*, 1997, vol. 36, p. 775.
15. R.W.K. Honeycombe: *Steels Microstructure and Properties*, Edward Arnold Ltd., London, 1981.
16. H.Y. Liou, R.I. Hsieh, and W.T. Tsai: *Materials Chemistry and Physics*, to be published.
17. H. Lee, C.H. Yoo, and H.M. Lee: *Mater. Technol.*, 1998, vol. 14, p. 54.